

ENHANCED MANEUVERABILITY BY ACTIVE VORTEX CONTROL WITH MOVEABLE BLOWING JET

X. Z. Huang and E.S. Hanff

Institute for Aerospace Research, National Research Council of Canada

Keywords: *vortex breakdown, active flow control, maneuverability*

Abstract

Water tunnel experiments were conducted on a 65° delta wing/centerbody half-model to explore the effectiveness of blowing into the leading-edge vortex through a moveable nozzle to control its breakdown. Tests conducted with the nozzle moving along the leading edge, wing surface and centerbody, revealed that the control power required to influence the breakdown process is a highly non-linear function of blowing location when the jet impinges on the vortex near its breakdown. The positive feedback implicit in the breakdown process is exploited to minimize the control mass flow required to position the breakdown at a desired location. Physical explanations are provided to explain the experimental observations. A novel concept, based on the above considerations, is proposed to enhance the maneuverability and controllability of advanced vehicles by using a moveable blowing jet impinging with a certain orientation at the optimum distance to the vortex breakdown location. Given the dominant effect of breakdown on airloads at high incidence and high angular rates, the proposed method can be used to control lift, pitching and rolling moment.

1 Introduction

The ability to manipulate flow field to obtain a desired effect on the airloads acting on an aircraft is of considerable technological importance. It is even more relevant in the case of the new generation of high-performance combat aircraft and the like as they typically rely on the leading-edge vortices to generate extra aerodynamic forces and control power in

order to expand their performance envelope and thus gain tactical advantage in combat. However, leading-edge vortex breakdown causes severe airload non-linearities and time dependence as well as highly unsteady flow downstream of the breakdown point. Active flow control concepts to control leading-edge vortex behavior is therefore of vital importance for enhancing maneuverability and controllability, and can, in principle, replace and/or complement conventional control surfaces, with their inherent limitations in the advanced maneuvering regime.

A number of methods have been and are being investigated which were described in a previous paper [1] and in a comprehensive survey conducted by Mitchell and Détery [2]. However, only limited success has been achieved so far in controlling leading-edge vortex behavior due to the unrealistically high control power requirements, low efficiency, complex mechanical arrangements and control methods, etc. For example, two methods, aft blowing at the apex and periodic blowing and suction along the leading-edge have been found to delay breakdown by 10% of centerline chord at a blowing momentum coefficient of 0.004 [2], [3]. Guillot et al employed high momentum coefficient of 0.013 that led to a delay of the breakdown location of up to 35 % centerline chord in some cases [4], [5]. The challenge remains on how to meet the control requirements in real applications with acceptable control power or engine bleed air and with a well behaved and simple transfer function that can be incorporated into control laws while being reasonably priced. From previous preliminary studies [1], it has been found that the required control power can be

largely reduced if the non-linear behaviour within the vortex breakdown region is fully understood and used. Thus additional studies were conducted over a wide range of conditions to further investigate the desired “sensitive spots” within the breakdown region and its response to a moveable blowing jet. Specifically, the effect of blowing into the breakdown region, while following its motion, was investigated over a range of angles of attack and compared with the effect of blowing at fixed locations far forward, aft or near the breakdown region. Some of the results and explanations are presented in this paper.

2 Experimental Set-Up

Experiments were conducted at the IAR 381 mm x 508 mm water tunnel with a vertical return circuit. The free-stream turbulence level in the tunnel is rated at $u/U_\infty < 1\%$ where U_∞ is the free stream velocity. Much care was exercised in ensuring that the turbulence screens were always free of trapped air bubbles and that a constant temperature of $22^\circ\text{C} \sim 24^\circ\text{C}$ was maintained.

A 65° delta wing or wing/centerbody half model and a reflection plate (horizontally oriented and located 50 mm below the water surface to avoid surface wave effects) are supported by a mechanism for changing the angle of attack. The centerline chord of the wing model is 228.6 mm.

Four experimental setups for controlling leading-edge vortex behavior were investigated. In the first one (Fig. 1a) the moveable blowing jet is applied along the leading edge by means of a wand with 1.0 mm inside diameter (ID), while in the second set-up (Fig. 1b) the blowing jet was applied through a nozzle of 0.71 mm ID connected to a tube that can be displaced along a dovetail shaped groove located under the vortex core on the upper wing surface. In the third set-up (Fig. 1c), where a centerbody has been added to the model, a nozzle, with the same ID as in the second case, can be moved along the fuselage. Finally, the fourth setup was used where the nozzle was located at the wing root in the absence of a centerbody (Fig.1d). In

all cases the nozzle aims back in the direction of an elevation angle of approximately 20° . The azimuthal angle of the nozzle was adjusted to obtain maximum effect on vortex breakdown.

To visualize the leading-edge vortex, dye was released from a 0.4 mm ID port located at 6.9% root chord near the leading edge on the windward model surface. In order to better visualize the effect of the blowing jet on the vortex, a second dye was released next to the blowing jet as shown in Fig. 1d.

The mass flow rate, $\dot{m} = a_j \rho_j U_j$, and momentum flow rate, $\dot{m} U_j = a_j \rho_j U_j^2$, are both important parameters where a_j and U_j are the jet area and velocity respectively. The former determines the mass consumption rate in a given application while the later is the blowing energy introduced into the flow field. For a given momentum rate the mass flow is proportional to the diameter of the blowing nozzle:

$$\frac{\dot{m}_1}{\dot{m}_2} = \frac{U_2}{U_1} = \frac{D_1}{D_2} \quad (1)$$

On the other hand, if the mass flow is the same, the momentum flow rate will be inverse proportional to the area of the blowing nozzle:

$$\frac{\dot{m}_1 U_1}{\dot{m}_2 U_2} = \frac{a_2}{a_1} = \left(\frac{D_2}{D_1}\right)^2 \quad (2)$$

Therefore in order to reduce the mass flow rate without reducing the momentum rate the nozzle diameter should be reasonable small. Nozzle diameters with the ID 1.0 mm and 0.71 mm respectively were used and the maximum momentum-blowing coefficient used in the experiment was 0.0029.

Tests were mostly conducted at a free stream velocity of 120 mm/sec, corresponding to a Reynolds number of 30,000. The tested angles of attack ranged from 22° to 42° , corresponding to vortex breakdown locations from the trailing edge to the apex in the absence of blowing.

The effect of blowing into the breakdown region while following its motion, was investigated over a range of angles of attack and compared with the effect of blowing at fixed locations far forward, aft or near the breakdown region. In addition, the influence of the wand

and nozzle -without blowing- on the vortex breakdown location was also investigated.

3 Experiment Results

The effect of the nozzle without blowing on the vortex breakdown location is shown in Figs. 2a (with no blowing tube) and 2b (with blowing tube, no blowing) and Figs. 3a (with no blowing tube) and 3b (with blowing tube, no blowing), corresponding to the first and second set-up respectively. The pictures show that there is virtually no effect on the breakdown location due to the presence of the blowing devices, which can thus be neglected.

Fig. 4 shows the effect of different but fixed blowing location on vortex breakdown for the first setup. Fig. 4a and Fig. 4b depict the effect of blowing far upstream of the breakdown location while Fig. 4c and Fig. 4d show the effect of blowing at a fixed location downstream of the naturally occurring breakdown location at two different times after the onset of blowing. When the blowing is applied far upstream of the breakdown location, the vortex is largely destroyed and it appears that the breakdown is promoted (compare Fig. 4a with Fig. 4b). When the breakdown is applied far downstream of the vortex breakdown, its effectiveness degrades as can be seen by comparing Fig. 4c and Fig. 4b. In this case, a much longer time is required for the breakdown to respond, as shown by Fig. 4c and Fig. 4d.

The most effective results to delay breakdown are obtained when the blowing location is displaced such that it follows the breakdown location as it progresses aft. In this case more than a 50% root chord delay can be achieved at a momentum-blowing coefficient of 0.0025.

For example, Fig. 5 shows that by properly applying the control jet to the breakdown location, the latter is delayed by approximately 0.2 c. If the wand is displaced aft such as to blow into the new location, the breakdown is once again delayed by approximately the same amount. Fig. 5a shows the initial flow conditions with the wand but no blowing, while Fig. 5b and Fig. 5c demonstrate the effect of

blowing. Fig. 6 uses double exposures to illustrate the vortex breakdown locations when the wand is continuously moving aft until breakdown crosses the trailing edge.

The experimental results showing the effect of the moveable blowing jet on breakdown location at different angles of attack are summarized in Fig. 7. Taking the amount of blowing rate into account, the effectiveness of this control method can be considerably higher than that of other approaches.

The moveable blowing experiments conducted at different spanwise locations, either at the leading edge, under the vortex core on the wing surface or along the fuselage (embodiment 1, 2 and 3 respectively), show nearly the same encouraging results. As examples, Fig. 8 and Fig 9 show the moveable blowing effect on vortex breakdown for the second and third embodiment respectively at even smaller blowing rates.

These results suggest that further studies could lead to a real application with acceptable blowing mass flow and power requirements.

In order to better investigate the effect of the blowing jet orientation on breakdown and the entrainment process, a secondary dye was introduced at a location next to that of the blowing jet. It is interesting to note that in the absence of the control jet, the entrainment of the secondary dye into the vortex can follow different spiral paths as shown in Fig. 10. When the secondary dye stream points below the vortex core the dye is drawn into the vortex as shown in Fig. 10a. Likewise, the secondary dye is pushed away from the vortex core as seen in Fig. 10b and Fig. 10c if it is released pointing towards or above the vortex core. It is worthwhile to point out that Fig. 10b and 10c were obtained under ostensibly the same test conditions, the cause for the differences in the behavior of the dye streak not being clear. Given the small momentum of the secondary dye stream, it is not clear whether its orientation or release location cause the above effects.

The effect of the control jet at different impingement transversal locations and orientations relative to the vortex axis on breakdown are shown in Fig. 11. The control

nozzle was located at the wing root (the forth setup). At the condition of the jet impinging under the vortex core, i.e. its spiral direction is the same as the vortex, the blowing is drawn into the vortex and the breakdown location is delayed (Fig. 11a). In contrast, when blowing is over the vortex core, i.e. its spiral direction is opposite to that of the vortex, the blowing jet is pushed away and the vortex breakdown is promoted (Fig. 11b). Similar attraction or rejection of the jet and its effect on vortex breakdown were observed for blowing along the leading-edge as shown in Fig. 12. If the blowing points above the vortex core it has the same spiral direction as that of the vortex, which results in delaying vortex breakdown location as shown in Fig. 12b.

4 Explanation and discussion

Given the complexity of truly three-dimensional vortex flows, the following discussion is first based on the assumption that the swirling flow is steady, inviscid and axisymmetric. The observed breakdown response is believed to be due to a non-linear behavior of the flow in the vicinity of the breakdown region which also comprises positive feedback mechanisms as pointed out by Brown and Lopez [6]. In general, leading-edge vortex breakdown depends on a balance of the vorticity feeding rate generated by the separation of the boundary layer at the leading edge and its downstream convection rate in the vortex (Lee and Ho [7]). At the location where the vorticity convection rate is less than the vorticity feeding rate, the vortex core is forced to tilt to maintain the total angular momentum in the vortex tube resulting in negative azimuthal vorticity. Brown and Lopez found that the tilted vortex and associated negative azimuthal vorticity introduce a negative axial velocity, increasing the adverse pressure gradient which in turn results in even more negative azimuthal vorticity. This positive feedback leads to the vortex core spiraling out and its diameter rapidly increasing, eventually breaking down into large-scale turbulence.

According to Brown and Lopez [6] the azimuthal vorticity on the stream surface is

$$\frac{\omega_\theta}{(\omega_\theta)_0} = \frac{r_0}{r} \left(\frac{\tan(\frac{U_\theta}{U_x})_0}{\tan(\frac{\omega_\theta}{\omega_x})_0} \right) - \frac{r}{r_0} \left(\frac{\tan(\frac{U_\theta}{U_x})_0}{\tan(\frac{\omega_\theta}{\omega_x})_0} - 1 \right) \quad (3)$$

where the subscript 0 indicates a location just upstream of breakdown and ω_θ , ω_x , and U_θ , U_x are azimuthal (tangential) and axial vorticity and velocity components respectively.

Fig. 13 illustrates the development of azimuthal vorticity under two different ratios, $k = \tan(\frac{U_\theta}{U_x})_0 / \tan(\frac{\omega_\theta}{\omega_x})_0 = 1$ and 2

For a given $(\omega_\theta)_0$, and $k \geq 1$, ω_θ becomes negative and diverges with increasing stream surface, r/r_0 . Under these conditions, the axial velocity, U_x , will decrease due to negative azimuthal vorticity since:

$$U_x(0, x) = \frac{1}{2} \int_{-\infty}^{\infty} \int_0^{\infty} \frac{r^2 \omega_\theta(r, \hat{x})}{[r^2 + (r - \hat{x})^2]^{\frac{3}{2}}} dr d\hat{x} \quad (4)$$

This reduced axial velocity, U_x , will further induce more negative azimuthal vorticity, ω_θ . If this positive feedback continues, this process eventually leads to the vortex breakdown.

In the case of a three-dimensional spiral vortex breakdown, the positive feedback is even stronger given that the vortex core does not rotate around its original axis as illustrated in Fig. 14. Applying angular momentum conservation in Ω_x , where x is defined along the intact vortex axis

$$\frac{1}{2} m r_c^2 \Omega_{x1} = \frac{1}{2} m r_c^2 \Omega_{x2} + m r^2 \Omega \quad (5)$$

if $\Omega = \frac{1}{3} \Omega_{x1}$ and $r = r_c$ then $\Omega_{x2} = \frac{1}{3} \Omega_{x1}$

which shows even larger reduction in angular velocity about the local spiraling vortex axis compared with an axisymmetric flow.

In order to find mechanisms to prevent the positive feedback in an axisymmetric swirling flow, one can resort to: Eq.(3) and the azimuthal vorticity transport equation shown below. For steady, inviscid and axisymmetric swirling flows, the azimuthal vorticity component is given by Batchelor and Darmofal [8],[9]:

$$\frac{D\omega_\theta}{Dt} = \left(\omega_r \frac{\partial U_\theta}{\partial r} \right)_t - \left(\frac{U_\theta \omega_r}{r} \right)_t + \left(\omega_x \frac{\partial U_\theta}{\partial x} \right)_t + \left(\frac{U_r \omega_\theta}{r} \right)_s \quad (6)$$

where subscripts “*t*” and “*s*” represent vortex tilting and stretching respectively. The first and second tilting terms correspond to the rotation of radial vorticity, ω_r , into the azimuthal direction while the third term represents the tilting of axial vorticity, ω_x , by an axial gradient of the swirl velocity, u_θ . Since in the vortex filament $\omega_x \gg \omega_\theta$ and $\omega_x \gg \omega_r$, the above equation can be further simplified as:

$$\frac{D\omega_\theta}{Dt} \approx \omega_x \frac{\partial U_\theta}{\partial x} \quad (7)$$

Blowing with an aft component into the vortex core in the breakdown region increases the local U_x , which according to Eq.(3) reduces the absolute value of negative azimuthal vorticity resulting in further recovery of axial velocity. Furthermore, if the blowing jet is oriented such that it introduces U_θ in the same rotational direction as the vortex, then $\frac{\partial U_\theta}{\partial x} > 0$ which also leads to a reduction in the absolute value of negative azimuthal vorticity, resulting in a decrease in k and forcing its value to be less than 1. These two facts will move breakdown aft of its original location.

The foregoing discussion demonstrates that, due to the above-mentioned positive feedback, the location of breakdown is particularly sensitive to perturbations in the flow in the region close to the vortex kink point. The effectiveness of blowing, e_b , largely depends on the radial distance of the impingement point of the blowing jet on the vortex and the distance to the latter’s breakdown location, $x_b - x_{1/B}$, blowing orientation and blowing rate, c_μ . As an example Fig. 15 illustrates the effectiveness of blowing for different axial distances at constant orientation with different blowing rate.

If blowing is applied far upstream of breakdown, where the flow is inherently very stable due to the absence of the above mentioned positive feedback, any realistically small amount of power added to the system by

the control jet is quickly distributed and dissipated without significantly altering the breakdown process. Likewise, if the blowing jet is applied far downstream of breakdown, a great deal of power and considerable time are required to reorganize the turbulent flow.

The aforementioned discussion is mostly limited to an axisymmetric vortex situation which may be true in low Reynolds number flow. At high Reynolds numbers the vortex flow is three-dimensional. Few examples in this area are known even for a single filament due to its complicated behavior. Therefore only a qualitative explanation, based on the propagation of weakly non-linear and non-axisymmetric waves on an incompressible and inviscid vortex, is given here for spiral vortex breakdown at high Reynolds number flow conditions.

Using an assumption of slow variations and the Local Induction approximation, Hasimoto has found that the solution of a thin vortex filament without stretching can be described by a non-linear Schrodinger equation[10]:

$$\frac{1}{i} \frac{\partial \psi}{\partial t} = \frac{\partial^2 \psi}{\partial s^2} + \frac{1}{2} (|\psi|^2 + A) \psi \quad (8)$$

where ψ is the complex variable:

$$\psi = \kappa \exp\left(i \int_0^s \tau ds\right) \quad (9)$$

while k and τ is the curvature and the torsion respectively. Hasimoto has found that this equation yields a solution describing the vortex filament which can be considered as the propagation of a wave packet of helical motion along a line vortex with a constant velocity 2τ . Its behavior depends on the value of k and τ and its motion can be decomposed into three parts: longitudinal motion U_x , rotation about the x -axis, ω_{rot} , and radial contraction and expansion, ω_{rad} . The faster motion of the larger looping seems to be coupled with the radial expansion by ω_{rad} , leading to the propagation of the solitary wave along the vortex filament. From that model, Leibovich [11] and Randall [12] further developed a weakly non-linear wave model for vortex breakdown. The vortex breakdown can be understood as changes from a super-critical state to a sub-critical one. Weak

disturbances, or waves, generated by a source located far downstream can propagate upstream up to the critical station. If the amplitude of the wave is not infinitesimally small, as is the case in most real cases, these waves can propagate a little beyond the critical station. At the same time, they are accelerated and amplified as shown by Schrödinger's equation. Similar to the axisymmetric case, the process of this acceleration and amplification results in a positive feedback. When their amplitude exceeds some critical value, these waves will become unstable to a spiral motion leading to vortex breakdown. On the basis of this qualitative discussion, applying energy into the breakdown region with the control jet can be expected to have similar effects as in the axisymmetric case, namely to reduce the accelerating and amplifying process so as to delay the breakdown.

It is worthwhile reiterating that the control jet can originate from any spanwise location, from the fuselage to the leading edge, with similar results. In real applications the former is probably more attractive due to the extra room available for installing the control devices.

5 A Novel Concept for Enhanced Maneuverability

Based on the experimental studies and the above discussion, a novel concept for controlling vortex breakdown location is suggested. The concept is based on: a) the determination of the required breakdown location as a function of existing conditions and pilot command in accordance with a desired control law and b) the adjustment of blowing location, orientation and rate to optimally force breakdown to the required location. Development of the concept requires the resolution of a variety of issues, such as its scalability and robustness in the presence of flow perturbations, development of fast, robust methods for the determination of breakdown location, design of suitable control loops, etc.

The whole system could be initially tested in a wind-tunnel experiment of a model such as that depicted in Fig. 16, which features several

pressure sensors and a moveable blowing nozzle that could be located along an arbitrary spanwise station. The pressure sensors are intended to detect the breakdown location. As vortex breakdown approaches, e.g. due to an angle of attack increase, the unsteady sensor signal becomes larger and its spectral content changes, information that is then used to adjust the blowing rate from the moveable blowing nozzle to ensure that breakdown remains behind it, thereby locking the breakdown location. Such an action could have a substantial effect on the maneuverability of an aircraft. In fact, it is estimated that in the case of a previously investigated 65° delta wing [13], breakdown control could lead to a maximum pitching and rolling moment coefficients of 0.05 with the control power obtained under realistic blowing coefficient.

Once the closed-loop method is shown to be capable of keeping breakdown where desired, the control flow can be applied sequentially through adjacent nozzles to force breakdown to an arbitrary position. Symmetric and differential shifting of the breakdown location can be used to control the normal force and rolling moment respectively.

The use of synthetic jets operating over a range of frequencies rather than constant blowing may also be investigated as a means to increase the proposed method's effectiveness. Finally, once a better understanding of the various system functions is acquired, the possibility of implementing a sensor-actuator system of MEMS could be considered (Fig. 17). Of course, considerable additional work is required before using the proposed approach under realistic conditions.

6 Conclusions

- There is positive feedback in the region of vortex breakdown. The effect of blowing on the delay of vortex breakdown is a non-linear function within that region.
- For any fixed blowing location, the delaying in breakdown is limited.

- By following the movement of breakdown, more than a 50% root chord delay in breakdown location can be achieved with acceptable blowing rates.
- The proposed concept of lock-in or control of vortex breakdown location has the potential advantage of high efficiency, simplicity and reasonable cost.
- Additional studies are required to verify the operation of the closed-loop system.

References

[1] Huang, X. and Hanff, E. A novel concept for controlling leading-edge vortex breakdown and related preliminary water tunnel experiment. AIAA Paper 2001-4143, 2001.

[2] Mitchell, A.M. and Délery, J. Research into Vortex Breakdown Control. *Progress in Aerospace Sciences* 37 (2001) 385-418, 2001.

[3] Mitchell, A. Barberis, D. and Molton, P. Experimental studies of control techniques for incompressible 3-d separation and vortex breakdown. AIAA 00-4415, 2000.

[4] Guillot, S., Gutmark, E.J. and Garrison, T.J. Delay of vortex breakdown over a delta wing via near-core blowing. AIAA Paper 98-0315

[5] Guillot, S. and Gutmark, E.J. Lift control of a delta wing by jet injection. AIAA paper 99-0137, 1999.

[6] Brown, G.L., and Lopez, J.M. Axisymmetric vortex breakdown. Part II Physical mechanisms. ARL-AERO-R-174.

[7] Lee, M. and Ho, C-M. Lift force of delta wings. *Applied mechanics Reviews*, Vol. 43, No. 9, 1990, pp. 209-221.

[8] Batchelor, G.K. *An Introduction to Fluid Dynamics*. Cambridge University Press, 1967.

[9] Darmofal, D.L. The role of vorticity dynamics in vortex breakdown. AIAA paper 93-3036, 1993.

[10] Hasimoto, H. A. Soliton on a vortex filament. *J. Fluid Mech.* (1972), Vol. 51, part 3, pp. 477-485.

[11] Leibovich, S. On a theoretical scenario for vortex breakdown. *Vortex Control and Breakdown Behavior, Second International Colloquium on Vortical Flows*, Switzerland, April 6-7, 1987.

[12] Randall, J.D. and Leibovich, S. The critical state: a trapped wave model of vortex breakdown. *J. Fluid Mech.* 58, 495-515

[13] Hanff, E.S. and Huang, X.Z. Highlights of the iar/wl high-alpha joint program. *NPU/AIAA/AFM Conference*, 1996.

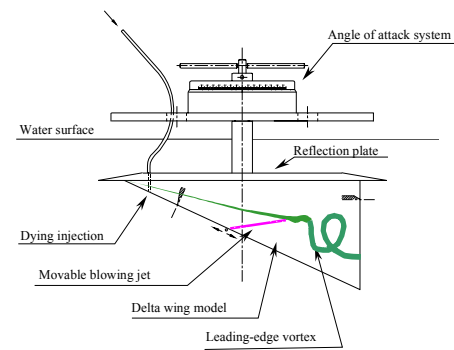


Fig. 1a blowing along leading-edge

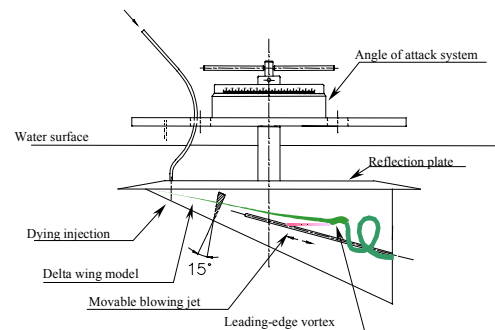


Fig. 1b blowing on the wing surface

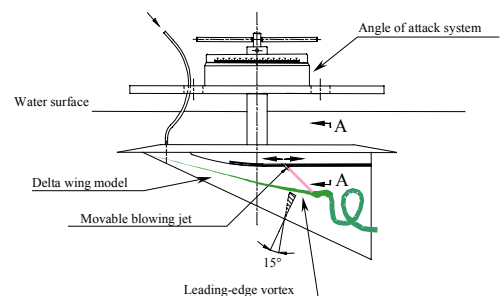


Fig. 1c blowing along the fuselage

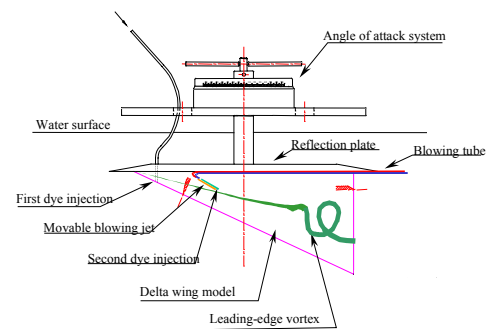
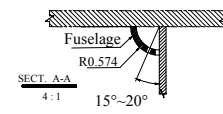


Fig. 1d blowing and two dyes set-up

Fig. 1 Experimental set-ups



2a no blowing tube 2b with tube no blowing

Fig. 2 Effect of blowing tube on vortex breakdown (first set-up, $\alpha=27^\circ$)



3a no blowing tube 3b with tube no blowing

Fig. 3 Effect of blowing tube on vortex breakdown (second set-up, $\alpha=22^\circ$)



4a far upstream blowing 4b no blowing tube



4c far downstream blowing $\Delta t=1\tau$ 4d far downstream blowing $\Delta t=2\tau$

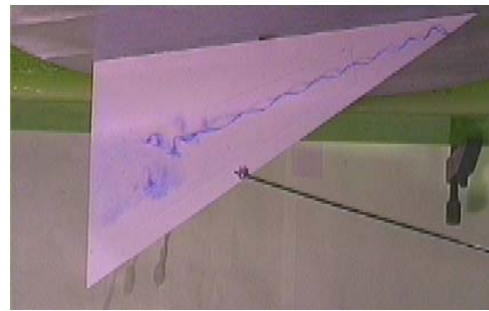
Fig. 4 Effect of different fixed blowing locations on vortex breakdown (first set-up, $C_\mu=0.0025$, $\alpha=27^\circ$)



5a initial station with no blowing

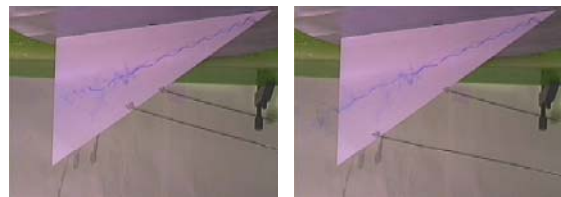


5b station 2



5c station 3

Fig. 5 Effect of moveable blowing jet on vortex breakdown at different fixed stations



6a

6b

Fig. 6 Double exposed images of moveable blowing jet effect on vortex breakdown

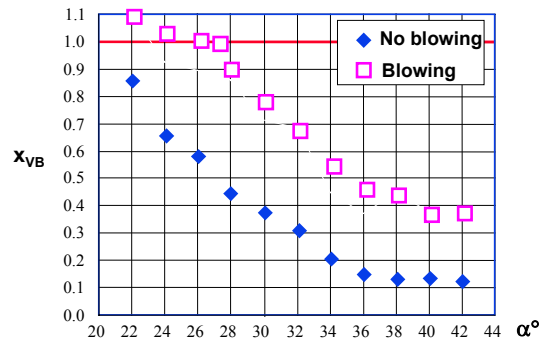


Fig. 7 Effects of moveable blowing on breakdown at different angles of attack



8a

8b



8c

8d

Fig. 8 Effects of moveable blowing on breakdown for second set-up at different locations ($C_\mu=0.0020$, $\alpha=27^\circ$)



9a no blowing



9b with moveable blowing

Fig. 9 Effects of moveable blowing on breakdown for third set-up ($C_{\mu}=0.0020$, $\alpha=25^\circ$)

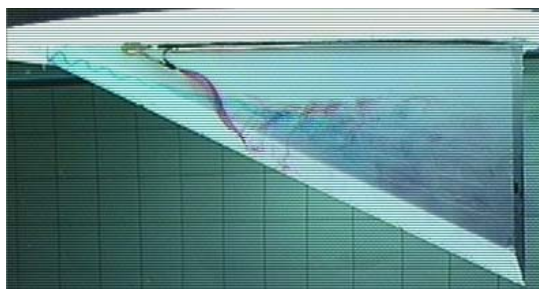


11a blowing under vortex core

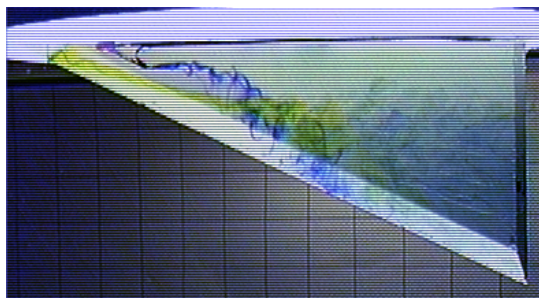


11b blowing over vortex core

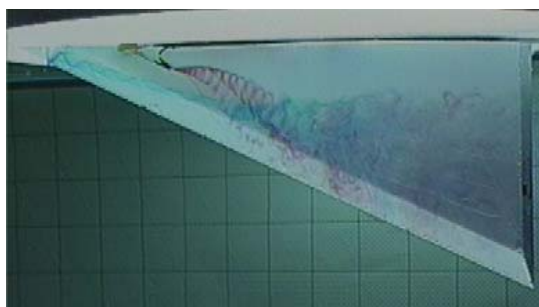
Fig. 11 Blowing effects at different orientations



10a spiral entrainment of secondary dye



10b repulsion entrainment of secondary dye



10c helix wave entrainment

Fig. 10 Different drawn-in status of second dye (no blowing)



12a blowing under vortex core



12b blowing over vortex core

Fig. 12 Blowing effects at different orientations for first set-up

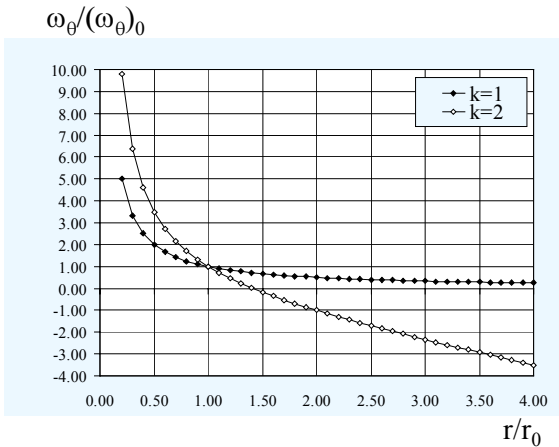


Fig. 13 Azimuthal vorticity vs. radius for different initial ratio of helix angles between velocity and vorticity

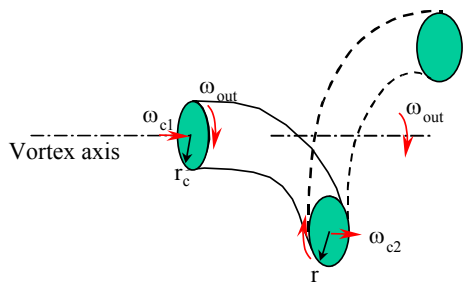


Fig. 14 Illustration of angular momentum conservation in spiral vortex breakdown region

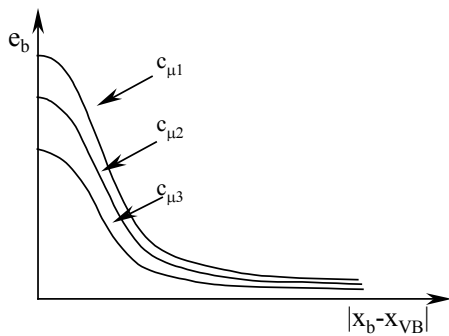
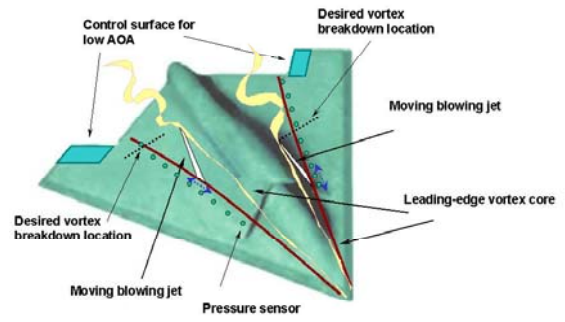
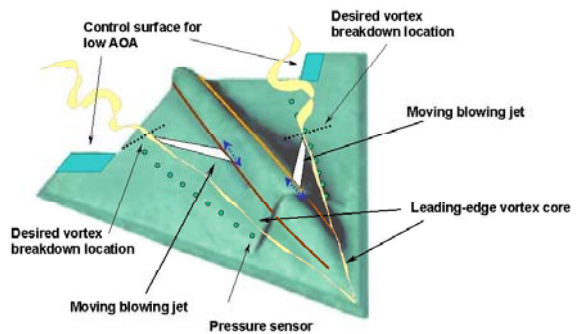


Fig. 15 Blowing efficiency vs. relative blowing location



16b blowing on the wing surface



16c blowing along fuselage

Fig. 16 A Novel concept of moveable blowing for controlling vortex breakdown

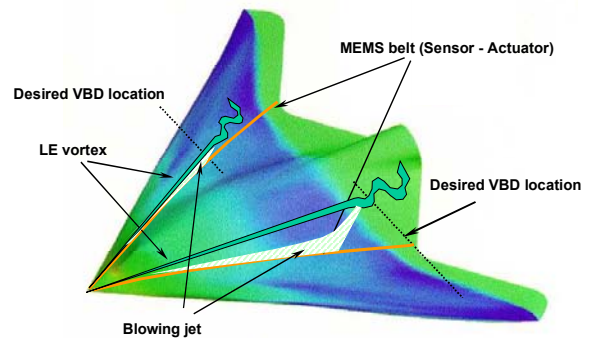
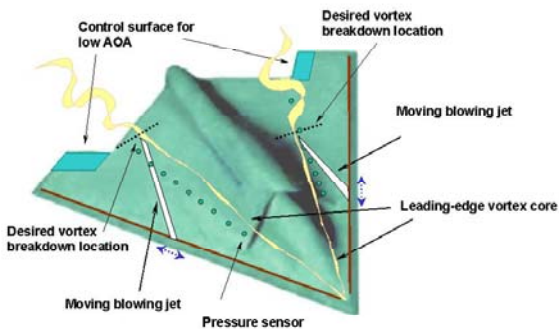


Fig. 17 Potential applications with MEMS



16a blowing along leading-edge